Journal of Zhejiang University-SCIENCE B 2026 27(1):89-100
www.jzus.zju.edu.cn; www.springer.com/journal/11585
E-mail: jzus_b@zju.edu.cn

Research Article
https://doi.org/10.1631/jzus.B2500069

Improving the thermal stability of *trans*-epoxysuccinate hydrolase

Wenna BAO[1], Jinfeng YAO[1], Haifeng PAN[2]✉, Ronglin ZHU[1], Xinying LI[1], Hongxiu LIAO[1]

[1]*School of Biological and Chemical Engineering, Zhejiang University of Science and Technology, Hangzhou 310023, China*
[2]*School of Life Sciences and Health, Huzhou College, Huzhou 313000, China*

Abstract: This study used molecular dynamics simulations, B-factor analysis, and saturation mutagenesis screening to enhance the thermal stability of the *trans*-epoxysuccinate hydrolase (TESH) derived from *Pseudomonas koreensis*. Eleven mutants that influence this characteristic were selected, yielding four mutants with improved activity. Among them, mutants A142C and S178Q exhibited lower Michaelis constant (K_m) values, and their k_{cat}/K_m ratios (k_{cat}, catalytic constant) were 3.7 and 0.9 times higher than those of the wild type, respectively. The values of half-life at 50 °C ($T_{1/2}^{50}$) of the two mutants were increased by 107% and 59%, respectively, compared to the wild type. Molecular docking and molecular dynamics simulations indicated that the two mutants showed stronger substrate interaction, lower binding energy, and reduced root mean square deviation compared to the wild type, along with decreased electrostatic potential energy and increased hydrophobicity near their mutation sites. The study of protein thermal stability engineering and associated mechanisms provides a valuable reference and holds practical significance for the industrial production of *meso*-tartaric acid.

Key words: *trans*-Epoxysuccinate hydrolase; *Pseudomonas koreana*; Molecular dynamics simulation; Thermal stability modification

1 Introduction

Epoxide hydrolases (EHs; EC 3.3.2.3), which are widely distributed in nature and present in organisms such as animals, plants, and microorganisms, require no cofactors to function. They are known to catalyze the enantioselective and regioselective addition of water molecules to the ethylene oxide ring of epoxides, resulting in optically active *o*-diols (Steinreiber and Faber, 2001). EHs from microbial sources are increasingly recognized as highly versatile biocatalysts for the preparation of enantiomeric pure epoxides and orthodiols, which form an important group of enantiomeric pure compounds in the chemical and pharmaceutical industries.

Epoxysuccinate hydrolase (ESH), a member of the EH family, can hydrolyze epoxysuccinic acid into tartaric acid (TA), serving as a key enzyme in the synthesis of TA (Archelas and Furstoss, 1998). Owing to the presence of two asymmetric carbon atoms, TA exists in three optical isomeric forms, including L(+)-TA, D(−)-TA, and *meso*-TA. The reported ESHs are primarily derived from bacteria (Sato and Yanai, 1976; Kamatani et al., 1977; Prescher and Schreyer, 1979; Rosenberg et al., 1999; Cheng et al., 2014), and their stereoselectivity varies across different sources. These three TA isomers are associated with the corresponding ESHs, which are designated as CESH[L] (*cis*-ESH for L(+)-TA production), CESH[D] (*cis*-ESH for D(−)-TA production), and TESH (*trans*-ESH for *meso*-TA production) (Sun et al., 2019). *meso*-TA is relatively rare, typically found as ferrous tartrate, and used as an anti-salt caking agent (Prescher and Schreyer, 1979). It also has applications in snow removal, baking powder preparation, and medicine (Bao et al., 2015).

Recently, we characterized TESH from *Pseudomonas koreensis* and explored its catalytic mechanism (Liao et al., 2024). However, when incubated at 45 °C for 30 min, only 10% of the residual activity of TESH remained, indicating its poor thermal stability. The modification of enzyme thermal stability not only improves enzyme performance but also enables effective application under a wide range of industrial scenarios

✉ Haifeng PAN, haifengpan518@163.com
Haifeng PAN, https://orcid.org/0000-0002-3585-372X

Received Feb. 9, 2025; Revision accepted May 12, 2025;
Crosschecked Nov. 14, 2025; Published online Dec. 22, 2025

and environments, playing a key role in many efficient and sustainable industrial processes. Bioinformatics are crucial in enzyme modification (Zhang et al., 2019). The B-factor is an important parameter in determining protein thermal stability. It reflects the movement and flexibility of atoms, amino acid side chains, and loop regions within protein structures. In general, a higher B-factor indicates greater atomic mobility and flexibility in a region, which corresponds to a more unstable structure; conversely, a lower B-factor suggests greater rigidity and structural stability (Tang et al., 2019; Carugo, 2022). Molecular dynamics simulations allow for the atomic-level simulation of protein systems, tracking the movement of molecules over time to uncover their dynamic properties. By simulating protein behavior under different conditions, such as variations in temperature, pH, or ligand binding, these simulations can provide insights into the factors influencing protein stability and help understand their effects on protein structure and function (Sinha et al., 2022; Weng et al., 2023).

In this study, molecular dynamics simulation was conducted to identify its unstable regions, and B-factor analysis helped pinpoint hotspots with poor thermal stability. Subsequently, saturation mutagenesis simulation was carried out to select and optimize stability-enhancing mutations. Eleven mutants were selected, mutated, and characterized, resulting in two mutants with improved thermal stability and enzymatic activity (Sakura et al., 2023). The findings provide an important reference for the thermal stability engineering of proteins and hold practical significance for the industrial production of *meso*-TA.

2 Materials and methods

2.1 Strains and plasmids

The TESH gene of *P. koreensis* (GenBank registration No. WP_151550555) was cloned in our laboratory and expressed in *Escherichia coli* BL21 (DE3)-pET15b(+)-TESH (Liao et al., 2024).

2.2 Homology modeling and molecular thermal stability simulation

The model of TESH was generated using the SWISS-MODEL (Waterhouse et al., 2018) (https://swissmodel.expasy.org), and B-factor analysis was conducted using HOTSOPT WIZARE v3.1 (Sumbalova et al., 2018) (https://loschmidt.chemi.muni.cz/hotspotwizard). Discovery Studio 2019 was utilized for mutant stability energy calculations and molecular dynamics simulations. The energy effect of each mutation on protein stability (mutation energy, $\Delta\Delta G_{mut}$) was calculated as the difference in folding free energy ($\Delta\Delta G_{folding}$) between the mutant structure and the wild-type protein, as expressed in Eq. (1):

$$\Delta\Delta G_{mut} = \Delta\Delta G_{folding\,(mutant)} - \Delta\Delta G_{folding\,(wild\text{-}type)}. \quad (1)$$

The folding free energy is defined as the difference in free energy between the folded and unfolded states of a protein, as expressed in Eq. (2):

$$\Delta\Delta G_{folding} = \Delta G_{fld} - \Delta G_{unf}, \quad (2)$$

where ΔG_{fld} and ΔG_{unf} represent the free energy of the folded and unfolded (denatured) states, respectively.

2.3 Construction of site-directed mutations

Taking the results of pre-screening as a basis, mutation primers were designed (Table S1). Site-directed mutagenesis was performed using PrimeSTAR® Max DNA polymerase (TaKaRa, Kyoto, Japan) and mutant primers, which were synthesized by Youkang Biological Company (Hangzhou, China).

2.4 Purification and characterization of enzymes

Wild-type and mutant TESHs were expressed in *E. coli* BL21 (DE3) cells and purified using His-Tag protein agarose purified resin (Sangon Biotech, Shanghai, China) according to the method for CESH[D] (Bao et al., 2014). After desalting the protein by ultrafiltration, 20% (volume fraction) glycerol was added at −20 °C for future use.

The effect of the thermal stability of TESH was investigated according to the method used for CESH[L] (Wang et al., 2013). The relative activity of the assay under standard reactions was set to 100%. The Michaelis constant (K_m), maximum reaction rate (V_{max}), and catalytic constant (k_{cat}) values of the enzyme were determined using the Michaelis-Menten plot when the concentration of *trans*-epoxysuccinic acid was increased from 20 to 320 mmol/L (Han et al., 2024). After incubating TESH at 50 °C for different periods, the temperature of the enzyme was adjusted to 37 °C

and the normalized conditions of pH 8.0 were set for 30 min to determine its stability.

2.5 Enzyme activity detection

The amount of *meso*-TA was determined by high-performance liquid chromatography (HPLC) on a chiral column (Chirex 3126 D-penicillanmin, 50 mm× 4.6 mm) at 60 ℃. The sample volume was 10 μL. The mobile phase consisted of 88% (volume fraction) 1 mmol/L copper acetate and 50 mmol/L ammonium acetate (pH 4.5) with 12% (volume fraction) isopropanol at a flow rate of 1 mL/min. Detection was performed at 280 nm (Cheng et al., 2014). TESH activity of one unit was defined as the amount of enzyme producing 1 μmol *meso*-TA per min at 37 ℃ and pH 8.0. Specific activity was defined as the number of units per milligram of protein. The protein concentration was determined by the Bradford Protein Assay Kit (Shanghai, China).

2.6 Molecular docking and molecular dynamics simulation

Molecular docking and molecular dynamics simulations were performed using the Discovery Studio 2019 client with CHARMM36 force field. The system was solvated in explicit water and subjected to a two-step energy minimization procedure. The first step was to perform energy minimization for 1000 steps, and the second step was to conduct energy minimization for 2000 steps. This was followed by a heating phase where the temperature was gradually increased from 50.00 K to 323.15 K, which was then maintained throughout both the equilibration and production stages. Production molecular dynamics simulations of 100 ns duration were conducted for both wild-type and mutant proteins with whole sequence at 323.15 K temperature and 1 bar (1 bar=1×10^5 Pa). Structural stability and flexibility were assessed by calculating root mean square deviation (RMSD) and root mean square fluctuation (RMSF) using the initial conformation as the reference (da Fonseca et al., 2024; Liao et al., 2024). For molecular docking, based on the previous research on the important active sites and catalytic mechanisms, the catalytic triad of Asp104-His272-Asp128 had been obtained (Liao et al., 2024). The region of this active center was selected for molecular docking, and the pose cluster radius was set to 0.1 nm.

3 Results and discussion

3.1 Homology modeling and dynamic simulation of TESH

The model used for molecular dynamics simulations was based on the 4NVR (putative acyltransferase from *Salmonella enterica*) template (Liao et al., 2024), with homologous modeling conducted using the SWISS-MODEL. The sequence similarity between the template and TESH was 52.43%. In the model assessment of SWISS-MODEL, the global model quality estimation (GMQE) value stood at 0.70, and the GMEAN value was 0.76±0.05 (Fig. S1). On the other hand, the conformational validity of the TESH homology model was evaluated using a Ramachandran plot (Fig. S2). This plot categorizes amino acid residues into four regions: most favored region (90.3%), allowed region (8.8%), generously allowed region (0.5%), and disallowed region (0.4%). For the assessment of homology models, the proportion of amino acids located in the disallowed region should be less than 5% of the total residues. Given this criterion, the constructed model exhibited high reliability and was deemed suitable for subsequent applications.

The simulation involved the pure protein under the CHARMM36 forcefield at 323.15 K (50 ℃) for 100 ns, during which the RMSD and RMSF values were calculated. The RMSD value serves as an indicator of protein stability, with lower RMSD values indicating reduced flexibility and greater stability. The simulations of wild-type TESH revealed that the RMSD initially increased during the first 25 ns and then fluctuated between 0.12 and 0.18 nm from 25 to 75 ns (Fig. 1a). However, after 75 ns, the RMSD began to rise steadily, suggesting that insufficient stability at 50 ℃.

RMSF values, which assess the flexibility of amino acid residues, identified regions with high flexibility that correlate with structural instability. As shown in Fig. 1b, the RMSF values were elevated in three red-highlighted regions, underscoring the critical role of these residues in the thermal stability of the enzyme.

3.2 Thermal stability analysis

The B-factor rankings of amino acid positions were calculated using HOTSPOT WIZARD v3.1, and the top 20 positions were selected for further analysis (Table S2). The B-factor reflects the thermal motion

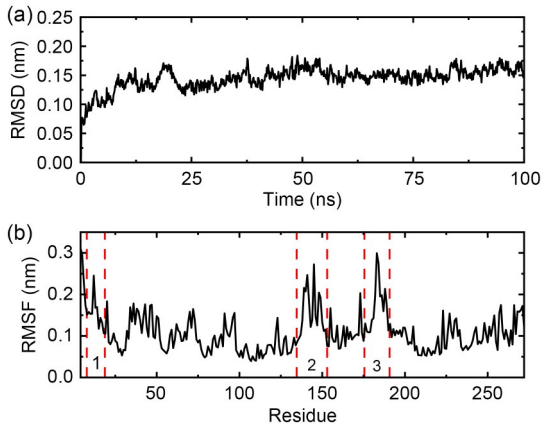

Fig. 1 Molecular dynamics simulation of wild-type *trans*-epoxysuccinate hydrolase (TESH). (a) Root mean square deviation (RMSD) values for wild-type TESH. (b) Root mean square fluctuation (RMSF) values for wild-type TESH.

or positional uncertainty of amino acid residues, with higher values indicating greater mobility or structural instability (Sun et al., 2019; Carugo, 2022). The results showed that the highest ranking positions were predominantly located in the second and third highlighted regions identified in the molecular dynamics simulation. These regions included residues in the hydrogen bond corners, α-helices, and loop regions (Table 1).

The RMSF reflects the time-averaged flexibility of residues in the solution state (dynamic environment), which can identify functionally critical dynamic regions (such as catalytic sites and allosteric regulatory regions). The B-factor characterizes the spatial disorder of residues in the crystalline state, primarily influenced by lattice packing and static conformations. The integrated analysis of both methods not only provides multi-scale validation spanning from dynamic simulations to static structural data but also enables the balanced optimization of rigidity enhancement and functional preservation in thermostability engineering, thereby offering a critical foundation for the rational design of mutation strategies.

Although the optimal temperature of wild-type enzyme was 50 ℃, its structural stability was significantly decreased. Therefore, residues in this region were subjected to saturation mutagenesis at 50 ℃. Stability assessments indicated that the mutation energy ($\Delta\Delta G_{mut}$) below −0.5 kcal/mol (1 kcal=4.184 kJ) was associated with a stable state. Based on these criteria, 11 mutants were selected for further investigation. Among them, R145I was considered neutral, while the remaining 10 showed enhanced stability. Although mutations in Q138I, N140I, and R145I led to reduced mutation energy, their stabilizing effects were less pronounced. In contrast, the other mutants exhibited significant improvements.

By combining B-factor analysis with molecular dynamics simulation results, the following 11 mutants were selected for further analysis: Q138I, T139W, N140I, A142C, A144F, R145I, S178Q, S180N, A181N, L183W, and K184L (Table 1). All of these residues were situated within the cap domain of the TESH structure (Fig. 2), which was consistent with the results by Taylor (1999), suggesting that the cap domain plays a crucial role in maintaining the overall structural stability.

B-factor analysis serves as a core tool for identifying thermolabile sites of an enzyme, and it is frequently integrated with other computational biology approaches to enhance the precision of a potential target. Han et al. (2019) identified the highly flexible region (residues 87-QNSS-90) in a fungal GH11 xylanase through B-factor analysis. By combining this

Table 1 Mutant B-factor ranking and mutational energy

Position	Secondary structure	B-factor ranking	Mutant	Mutation energy (kcal/mol)
Q138	Hydrogen-bonded turn	9	Q138I	−0.87
T139	Loop	7	T139W	−2.18
N140	Loop	4	N140I	−0.68
A142	α-Helix	3	A142C	−1.06
A144	α-Helix	8	A144F	−1.38
R145	α-Helix	11	R145I	−0.30
S178	Hydrogen-bonded turn	6	S178Q	−1.28
S180	Hydrogen-bonded turn	2	S180N	−1.33
A181	Hydrogen-bonded turn	1	A181N	−1.22
L183	Hydrogen-bonded turn	5	L183W	−2.41
K184	Hydrogen-bonded turn	10	K184L	−2.40

1 kcal=4.184 kJ.

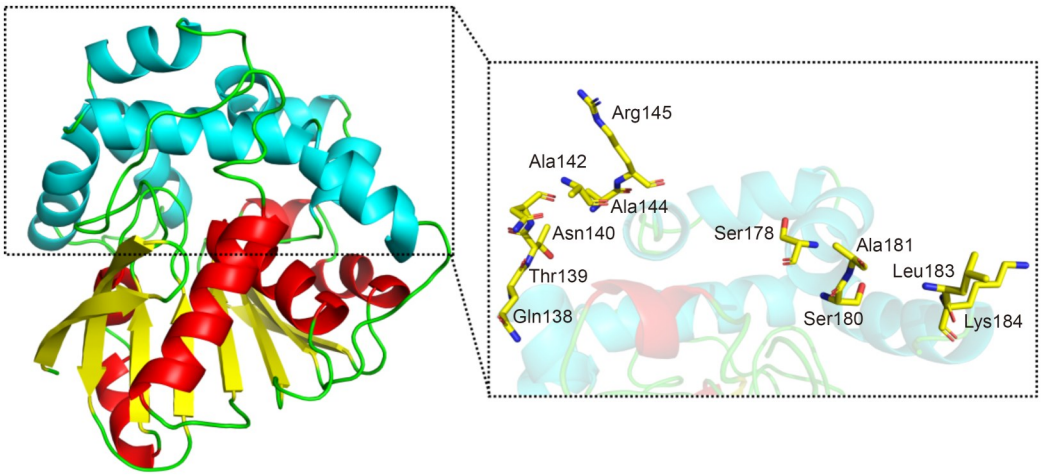

Fig. 2 Molecular dynamics simulation of wild-type *trans*-epoxysuccinate hydrolase (TESH). The cap domain is composed of α-helices (marked in blue), and the core domain consists of α-helices (marked in red) and β-sheets (marked in yellow). Other secondary structures were marked in green. The 11 thermostability-related residues to be modified were shown.

with multiple sequence alignment, they observed that homologous thermophilic enzymes exhibited conserved residues 87-RGHT-90 at this site. Therefore, four single mutants (Q87R, N88G, S89H, and S90T) were constructed, all of which showed significantly improved thermostability. Zhu et al. (2022) further expanded this strategy in engineering the thermostability of glutathione bifunctional synthase from *Streptococcus agalactiae* (GshFSA). By coupling B-factor-screened high-fluctuation residues with unfolding free energy calculations, they obtained mutants R270S and Q406M with 2.62-fold and 3.02-fold increases in half-life period compared to the wild type, respectively. In this study, we integrated B-factor analysis with full-atom molecular dynamics simulations, employing dual criteria—static flexibility (B-factor) and dynamic fluctuations (RMSF), yielding the identification of 11 high-confidence thermolabile residues. This highlights the superior efficacy of integrating static and dynamic analyses in thermostability engineering.

3.3 Characterization of mutants

Site-directed mutagenesis by polymerase chain reaction (PCR) was carried out, and its PCR products (Fig. S3) were transferred into *E. coli* BL21 (DE3) for expression. The wild-type and mutant TESHs were purified using nickel affinity chromatography, with the results shown in Fig. 3. The bands of all mutants were relatively single, indicating high purity. The expression level of target protein varies across different mutants and the expression of mutant Q138I was the lowest. Kinetic analysis of each mutant showed that Q138I, T139W, and A144F nearly lost enzyme activity (Table 2). Conversely, mutants A142C, R145I, S178Q, and K184L displayed enhanced activity compared to the wild type, while the remaining mutants also decreased to varying degrees. Notably, A142C and S178Q exhibited lower K_m values than the wild type, indicating an improved affinity for the substrate. In contrast, most of the other mutants showed an increase in K_m values. The catalytic efficiency, represented by the k_{cat}/K_m ratio, was higher for A142C, S178Q, S180N, and K184L compared to the wild type, further underscoring their enhanced performance.

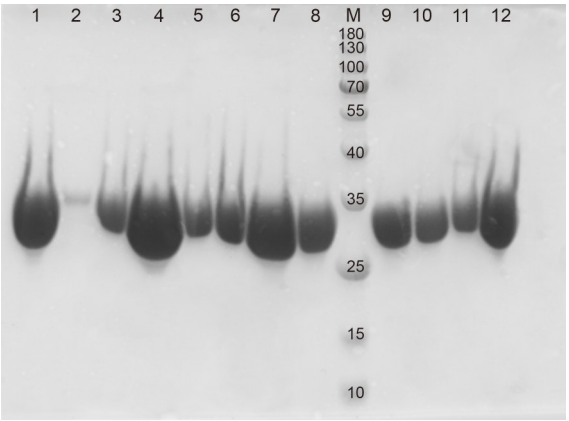

Fig. 3 Sodium dodecyl sulfate-polyacrylamide gel electrophoresis (SDS-PAGE) analysis of purified *trans*-epoxysuccinate hydrolases (TESHs). Lanes: (1) wild type; (2) Q138I; (3) T139W; (4) N140I; (5) A142C; (6) A144F; (7) R145I; (8) S178Q; (9) S180N; (10) A181N; (11) L183W; (12) K184L; (M) protein marker (kDa).

Table 2 Characterization of wild-type and mutant TESHs

Enzyme	Relative activity (%)*	K_m (mmol/L)	k_{cat} (s^{-1})	k_{cat}/K_m (mmol/(L·s))	$T_{1/2}^{50}$ (min)
Wild type	100.00±1.40	72.27	294.30	4.07	29.5
Q138I	4.03±0.19	n.a.	n.a.	n.a.	n.a.
T139W	4.73±1.20	n.a.	n.a.	n.a.	n.a.
N140I	29.80±1.27	507.60	501.94	0.99	6.0
A142C	130.77±1.43	25.40	486.74	19.16	61.0
A144F	1.73±0.05	n.a.	n.a.	n.a.	n.a.
R145I	179.07±1.85	130.20	76.52	0.59	3.5
S178Q	131.56±2.17	63.46	495.93	7.81	47.0
S180N	72.90±1.47	95.95	473.08	4.93	4.5
A181N	66.56±1.72	149.80	285.23	1.90	51.0
L183W	8.71±1.77	n.a.	n.a.	n.a.	n.a.
K184L	286.30±1.67	75.93	587.55	7.74	15.0

The enzyme activity of wild-type *trans*-epoxysuccinate hydrolase (TESH) is 147.78 μmol/(min·mg). n.a.: not assayed due to low enzyme activity.
* Data are expressed as mean±standard deviation (SD), n=3. K_m: Michaelis constant; k_{cat}: catalytic constant; $T_{1/2}^{50}$: half-life at 50 °C.

3.4 Analysis of thermal stability

The specific activity of the wild-type and mutant TESHs after different incubation time was shown in Fig. 4. The enzyme activity of the wild-type TESH gradually declined in the first 60 min, losing most of its activity during the period. Among the mutants, under the initial conditions of reaction at 37 °C for 30 min, the enzyme activity of A142C, R145I, S178Q, S180N, and K184L mutants was higher than that of the wild type. After incubation at 50 °C for 15 min, the enzyme activity of R145I, S180N and K184L decreased significantly, falling below that of the wild type, indicating no improvement in thermal stability. In contrast, mutants A142C and S178Q exhibited higher initial enzyme activity than the wild type; their residual enzyme activity remained consistently higher with increasing time, showing a notable enhancement in thermal stability.

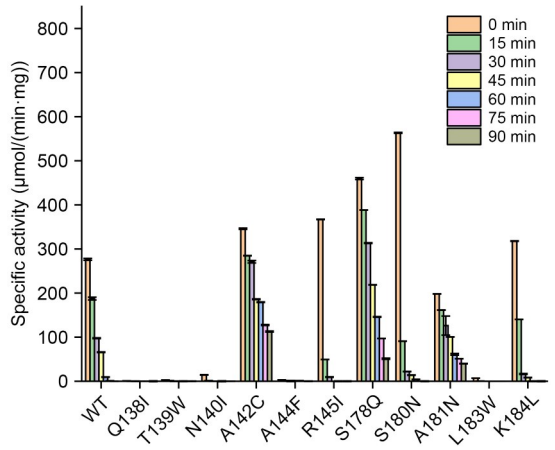

Fig. 4 Specific activity of the wild-type and mutant *trans*-epoxysuccinate hydrolases (TESHs) at different incubation times. Data are expressed as mean±standard deviation (SD), n=3.

The residual enzyme activity of the wild-type and mutant TESHs at various time is shown in Fig. S4. The results indicate that the half-life at 50 °C ($T_{1/2}^{50}$) values of A142C and S178Q increased by 107% and 59%, respectively, compared to the wild type. Among these two mutants, S178Q displayed better thermal stability during the first 45 min of incubation at 50 °C. However, after 45 min, A142C showed superior thermal stability, retaining 40% of its enzyme activity after incubation for 90 min, while the wild-type TESH showed a significant decline. Although the initial enzyme activity of A181N was lower than that of the wild type, its $T_{1/2}^{50}$ increased by 73% after incubation for 90 min, with only a slight reduction in enzyme activity, indicating good thermal stability for this mutant (Table 2).

3.5 Molecular docking

Molecular docking of the wild-type and mutant TESHs with the substrate (*trans*-epoxysuccinate) was performed. We selected the top-ranked conformation based on comprehensive scoring from the docking site heat map, which demonstrated higher confidence levels at multiple amino acid sites compared to other conformations (Fig. S5). The reliability of docking sites was further evaluated by calculating both the radius of gyration (R_g) and Jurs solvent accessible surface area (Jurs_SASA) values (Table S3). The R_g value

reflects the relationship between conformational flexibility and spatial complementarity (Bhonsle et al., 2007), where lower values indicate more efficient conformational sampling and higher reliability. Jurs_SASA characterizes solvation effects and surface interactions, and a lower Jurs_SASA value suggests that the conformation may have formed a tighter binding interface (e.g., a hydrophobic pocket), resulting in reduced solvent exposure. Notably, both the R_g and Jurs_SASA values of the selected conformations were below average.

The docking energy was also calculated (Table S4). Except for certain mutants that largely lost enzyme activity and A181N, the binding energy of the remaining mutants decreased. Lower binding energy indicates a closer interaction between the enzyme and the substrate, leading to a more effective reaction, aligning well with the experimental results. For A181N, the binding energy showed minimal change compared to the wild-type enzyme, consistent with its reduced activity observed in experiments. In the calculation of docking interaction energy, all six mutants exhibited decreased values. Notably, the mutants A142C and S178Q, which showed significant experimental improvements, also displayed substantial reductions in binding energy.

The docking results of the wild type and mutants A142C, S178Q, and A181N with substrate molecules are shown in Fig. 5. Compared to the wild type, the A142C mutant showed shorter bond lengths at several amino acid sites, indicating a closer interaction with the substrate. For example, the bond length at the Arg105 site was reduced from 0.520 to 0.417 nm, enhancing the attractive charge interaction to form a salt bridge. In addition, Arg108 formed a new conventional hydrogen bond with a bond length of 0.452 nm, which plays a key role in improving thermal stability (Hendsch and Tidor, 1994; Ban et al., 2021). Similarly, the S178Q mutant also showed varying degrees of bond-length reduction in its interactions. At the Arg105 site, the bond length decreased from 0.520 nm to

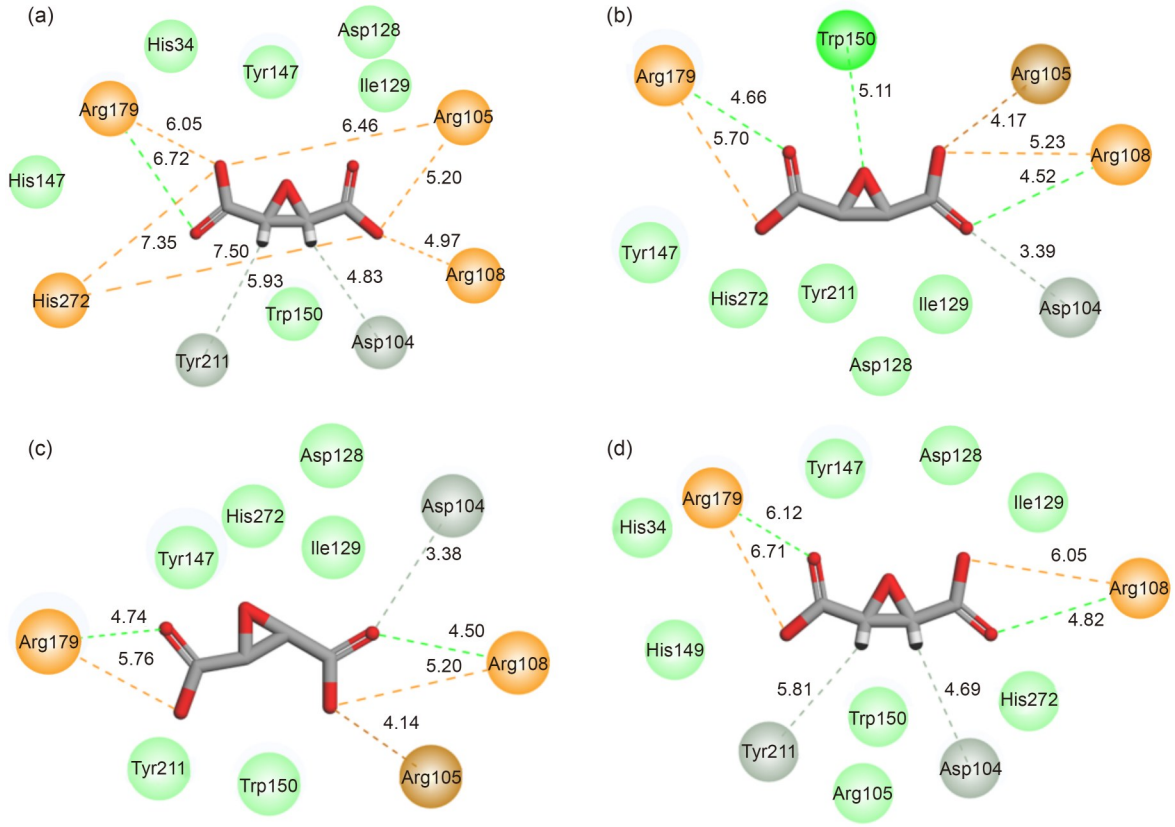

Fig. 5 Interaction of substrate-binding sites. The amino acids near the binding pocket are shown and their interactions with substrate are represented by different colors. Light green represents van der Waals forces, dark green represents hydrogen bonds, dark brown represents salt bridges, light gray represents carbon hydrogen bonds, and orange represents charge interactions. (a) Wild type; (b) A142C; (c) S178Q; (d) A181N.

0.414 nm, and this interaction was also enhanced to form a salt bridge. Arg108 formed an additional conventional hydrogen bond with a bond length of 0.450 nm. These docking results corroborate the observed experimental improvements in the thermal stability of A142C and S178Q. In contrast, the docking results for A181N did not show significant differences from the wild-type TESH. Notably, the Arg105 site did not participate in the reaction.

In summary, molecular docking indicated that the binding energy of the mutants A142C and S178Q decreased, the bond length of the interaction was shortened to varying degrees, and the binding to the substrate was closer. The Arg105 amino acid sites were all enhanced in the original attractive charge interaction force as a salt bridge, which played an important role in the thermal stability of the enzyme.

3.6 Molecular dynamics simulation of mutants

Molecular dynamics simulations were performed to calculate and compare the RMSD (Fig. 6) and RMSF (Fig. 7) values of the wild-type and mutant variants, enabling a quantitative analysis of the effects of mutations on the structural stability and dynamic flexibility of TESH. The RMSD value is inversely correlated with protein stability: lower RMSD values indicate reduced flexibility, signifying a more stable protein structure, which is consistent with our experimental results. Among the three mutants (A142C, S178Q, and A181N) that showed improved thermal stability in the experiments, their RMSD values decreased to varying extents compared with those of the wild type, indicating enhanced stability (Fig. 6). These findings align with and confirm the experimental results.

Next, comparative analyses of the RMSF values between the wild type and three thermostable mutants (A142C, S178Q, and A181N) were carried out (Fig. 7). The mutant A142C exhibited reduced RMSF values around residue 142 compared to the wild type. Similarly, both S178Q and A181N showed decreased RMSF values near residue 180. These observed reductions in RMSF values suggested decreased conformational flexibility in these regions, making the structure more stable.

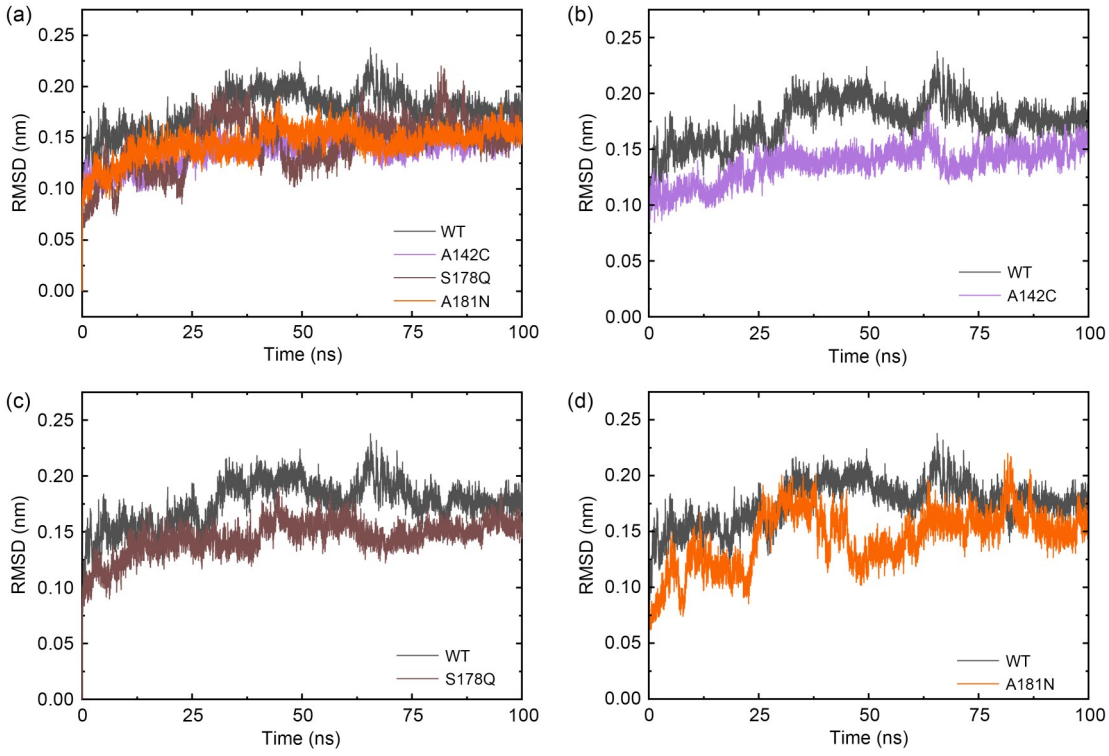

Fig. 6 Root mean square deviation (RMSD) values of the wild-type (WT) and mutant *trans*-epoxysuccinate hydrolases (TESHs). (a) Comparison of the RMSD values between the wild type (WT) and three mutant TESHs. (b) Comparison of the RMSD values between the wild type (WT) and mutant A142C. (c) Comparison of the RMSD values between the wild type (WT) and mutant S178Q. (d) Comparison of the RMSD values between the wild type (WT) and mutant A181N.

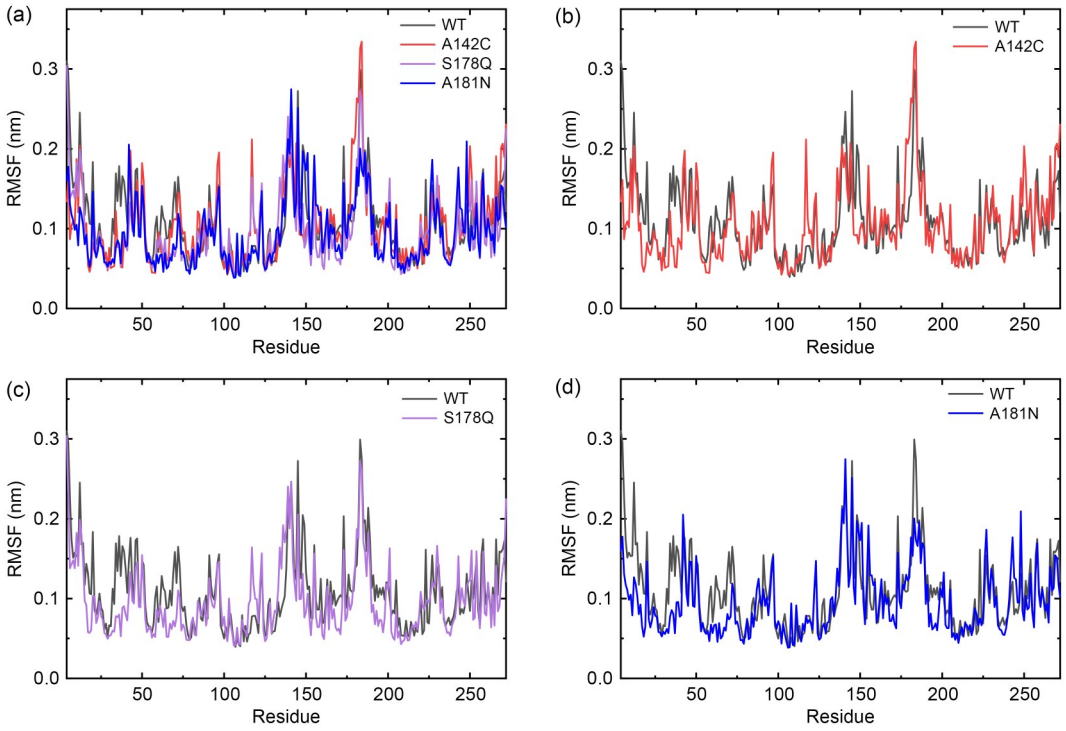

Fig. 7 Root mean square fluctuation (RMSF) values of the wild-type (WT) and mutant *trans*-epoxysuccinate hydrolases (TESHs). (a) Comparison of the RMSF values between the wild type (WT) and three mutant TESHs. (b) Comparison of the RMSF values between the wild type (WT) and mutant A142C. (c) Comparison of the RMSF values between the wild type (WT) and mutant S178Q. (d) Comparison of the RMSF values between the wild type (WT) and mutant A181N.

The analysis of electrostatic potential energy in the three mutants (Fig. 8) revealed varying degrees of reduction, with A142C exhibiting the lowest values. Surface-charged groups play a crucial role in the structure and function (such as stability) of proteins (Stigter et al., 1991). Our results suggested that mutants with less positive charge in the mutated region possess enhanced thermal stability. Concurrently, hydrophobic interactions mediated by van der Waals forces contribute to structural stabilization by forming robust internal frameworks that resist environmental perturbations (e.g., temperature or pH fluctuations), thereby preserving the native conformation and biological activity of the enzyme. While the A142C mutation site itself showed minimal changes, its surrounding regions displayed enhanced hydrophobicity, whereas S178Q and A181N exhibited direct hydrophobicity increases at their mutation sites, likely contributing to the observed thermal stability improvement (Fig. 9).

The above findings demonstrate that single amino acid mutations could significantly alter enzymatic functional properties through multiple mechanisms. These structural mutations may modify the charge distribution and microenvironment of the active site, regulate

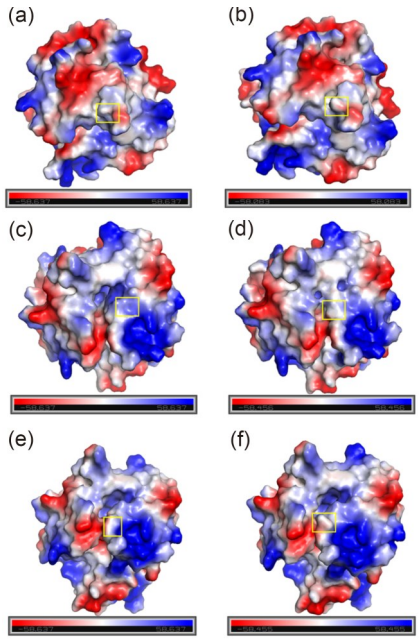

Fig. 8 Comparison of surface electrostatic energy between the wild type and mutants. The red regions represent negative charges, whereas the blue regions denote positive charges. The red-to-blue color gradient illustrates the continuous transition of charge from negative to positive properties. (a) Wild type (vs. A142C); (b) A142C; (c) wild type (vs. S178Q); (d) S178Q; (e) wild type (vs. A181N); (f) A181N.

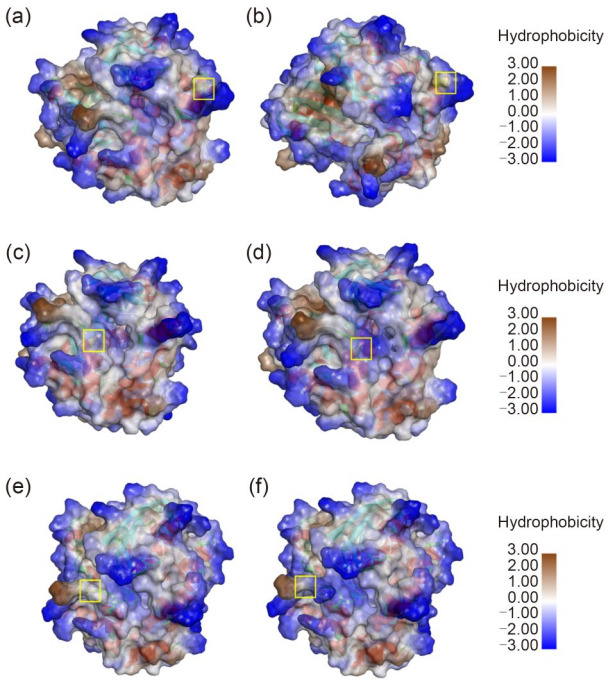

Fig. 9 Comparison of surface hydrophobic interactions between the wild type and mutants. The blue regions represent hydrophobic areas, while the brown regions denote hydrophilic zones. The blue-to-brown color gradient illustrates the continuous transition from hydrophobic to hydrophilic characteristics. (a) Wild type (vs. A142C); (b) A142C; (c) wild type (vs. S178Q); (d) S178Q; (e) wild type (vs. A181N); (f) A181N.

the dynamic flexibility of protein conformation, or affect the spatial accessibility of substrate-binding channels, subsequently leading to functional alterations, such as changes in substrate selectivity (e.g., variations in K_m values) and inhibitor sensitivity. This underscores the "single-site mutation→conformational adaptation→functional alteration" cascade mechanism in protein structures, establishing a theoretical framework for the comprehension and prediction of how mutations influence enzymatic function.

4 Conclusions

In this work, bioinformatics methods were used to enhance the thermal stability of the TESHs from *P. koreensis*. Molecular dynamics simulations identified three unstable regions in the wild-type TESH. Combining B-factor analysis and saturation mutagenesis screening, 11 sites that influence the thermal stability of the enzyme were selected, all of which were located in the cap domain. Four mutants with improved enzyme activity were obtained (A142C, R145I, S178Q, and K184L). Among them, mutants A142C and S178Q exhibited lower K_m values than the wild type, and their k_{cat}/K_m ratios were 3.7 and 0.9 times higher than those of the wild type, respectively, indicating that they got higher catalytic efficiency. The thermal stability experiment showed that the $T_{1/2}^{50}$ values of mutants A142C and S178Q were 1.1 and 0.6 times higher than that of the wild type, respectively. Furthermore, although the initial enzyme activity of the mutant A181N was lower than that of the wild-type enzyme, its thermal stability was improved. Molecular docking analysis showed that the binding energy of mutants A142C and S178Q with the substrate decreased, while new salt bridges were formed, which played a crucial role in the stability of the protein. Molecular dynamics simulations revealed that the RMSD and RMSF (around mutation sites) values of these two mutants were significantly lower than those of the wild type. The three thermostable mutants exhibited varying degrees of reduced electrostatic potential energy and increased hydrophobicity in the vicinity of their mutation sites. The above findings provide a valuable reference for the thermal stability engineering of proteins, and hold practical significance for the industrial production of *meso*-TA.

Data availability statement

The dataset used or analyzed during the current study is available from the corresponding author upon reasonable request.

Acknowledgments

This work was supported by the Scientific Research Fund of Zhejiang Provincial Education Department (No. Y202248484) and the Huzhou Science and Technology Plan Project (No. 2022GZ56), China.

Author contributions

Wenna BAO contributed to the conceptualization, supervision, experimental design, and writing. Jinfeng YAO contributed to the data curation and writing – original draft. Haifeng PAN performed the data curation, reviewed and edited the manuscript, and obtained the funding support. Ronglin ZHU, Xinying LI, and Hongxiu LIAO contributed to experimental research and data analysis. All authors have read and approved the final manuscript, and therefore, have full access to all the data in the study and take responsibility for the integrity and security of the data.

Compliance with ethics guidelines

Wenna BAO, Jinfeng YAO, Haifeng PAN, Ronglin ZHU, Xinying LI, and Hongxiu LIAO declare that they have no conflicts of interest.

This article does not contain any studies with human or animal subjects performed by any of the authors.

References

Archelas A, Furstoss R, 1998. Epoxide hydrolases: new tools for the synthesis of fine organic chemicals. *Trends Biotechnol*, 16(3):108-116. https://doi.org/10.1016/S0167-7799(97)01161-X

Ban XF, Xie XF, Li CM, et al., 2021. The desirable salt bridges in amylases: distribution, configuration and location. *Food Chem*, 354:129475. https://doi.org/10.1016/j.foodchem.2021.129475

Bao WN, Pan HF, Zhang ZH, et al., 2014. Analysis of essential amino acid residues for catalytic activity of *cis*-epoxysuccinate hydrolase from *Bordetella* sp. BK-52. *Appl Microbiol Biotechnol*, 98(4):1641-1649. https://doi.org/10.1007/s00253-013-5019-2

Bao WN, Pan HF, Zhang ZH, et al., 2015. Isolation of the stable strain *Labrys* sp. BK-8 for L(+)-tartaric acid production. *J Biosci Bioeng*, 119(5):538-542. https://doi.org/10.1016/j.jbiosc.2014.10.013

Bhonsle JB, Venugopal D, Huddler DP, et al., 2007. Application of 3D-QSAR for identification of descriptors defining bioactivity of antimicrobial peptides. *J Med Chem*, 50(26):6545-6553. https://doi.org/10.1021/jm070884y

Carugo O, 2022. *B*-factor accuracy in protein crystal structures. *Acta Crystallogr Sect D Struct Biol*, 78(1):69-74. https://doi.org/10.1107/S2059798321011736

Cheng YQ, Wang L, Pan HF, et al., 2014. Purification and characterization of a novel *cis*-epoxysuccinate hydrolase from *Klebsiella* sp. that produces L(+)-tartaric acid. *Biotechnol Lett*, 36(11):2325-2330. https://doi.org/10.1007/s10529-014-1614-2

da Fonseca AM, Caluaco BJ, Madureira JMC, et al., 2024. Screening of potential inhibitors targeting the main protease structure of SARS-CoV-2 via molecular docking, and approach with molecular dynamics, RMSD, RMSF, H-bond, SASA and MMGBSA. *Mol Biotechnol*, 66(8):1919-1933. https://doi.org/10.1007/s12033-023-00831-x

Han JY, Ding YJ, Wei QN, et al., 2024. Expression and characterization of a bifunctional glycoside hydrolase IDSGH5-23 from *Ruminococcus albus*. *J Zhejiang Univ (Agric Life Sci)*, 50(6):963-972. https://doi.org/10.3785/j.issn.1008-9209.2023.09.281

Han NY, Ma Y, Mu YL, et al., 2019. Enhancing thermal tolerance of a fungal GH11 xylanase guided by B-factor analysis and multiple sequence alignment. *Enzyme Microb Technol*, 131:109422. https://doi.org/10.1016/j.enzmictec.2019.109422

Hendsch ZS, Tidor B, 1994. Do salt bridges stabilize proteins? A continuum electrostatic analysis. *Protein Sci*, 3(2):211-226. https://doi.org/10.1002/pro.5560030206

Kamatani Y, Okazaki H, Imai K, et al., 1977. Production of L(+)-tartaric acid. US Patent 4011135A.

Liao HX, Pan HF, Yao JF, et al., 2024. Essential amino acid residues and catalytic mechanism of *trans*-epoxysuccinate hydrolase for production of *meso*-tartaric acid. *Biotechnol Lett*, 46(5):739-749. https://doi.org/10.1007/s10529-024-03490-3

Prescher G, Schreyer G, 1979. Process for the production of pure racemic acid and mesotartaric acid and separation of maleic acid from synthetic tartaric acid. US Patent 4150241A.

Rosenberg M, Miková H, Krištofíková L, 1999. Production of L-tartaric acid by immobilized bacterial cells *Nocardia Tartaricans*. *Biotechnol Lett*, 21(6):491-495. https://doi.org/10.1023/A:1005592104426

Sato E, Yanai A, 1976. Method for preparing D-tartaric acid. US Patent 3957579A.

Sakura K, Esther W, Darshan S, et al., 2023. Genetic resources and precise gene editing for targeted improvement of barley abiotic stress tolerance. *J Zhejiang Univ-Sci B (Biomed & Biotechnol)*, 24(12):1069-1092. https://doi.org/10.1631/jzus.B2200552

Sinha S, Tam B, Wang SM, 2022. Applications of molecular dynamics simulation in protein study. *Membranes*, 12(9):844. https://doi.org/10.3390/membranes12090844

Steinreiber A, Faber K, 2001. Microbial epoxide hydrolases for preparative biotransformations. *Curr Opin Biotechnol*, 12(6):552-558. https://doi.org/10.1016/S0958-1669(01)00262-2

Stigter D, Alonso DO, Dill KA, 1991. Protein stability: electrostatics and compact denatured states. *Proc Natl Acad Sci USA*, 88(10):4176-4180. https://doi.org/10.1073/pnas.88.10.4176

Sumbalova L, Stourac J, Martinek T, et al., 2018. HotsPot Wizard 3.0: web server for automated design of mutations and smart libraries based on sequence input information. *Nucleic Acids Res*, 46(W1):W356-W362. https://doi.org/10.1093/nar/gky417

Sun ZT, Liu Q, Qu G, et al., 2019. Utility of B-factors in protein science: interpreting rigidity, flexibility, and internal motion and engineering thermostability. *Chem Rev*, 119(3):1626-1665. https://doi.org/10.1021/acs.chemrev.8b00290

Tang H, Shi K, Shi C, et al., 2019. Enhancing subtilisin thermostability through a modified normalized B-factor analysis and loop-grafting strategy. *J Biol Chem*, 294(48):18398-18407. https://doi.org/10.1074/jbc.RA119.010658

Taylor WR, 1999. Protein structural domain identification. *Protein Eng Des Sel*, 12(3):203-216. https://doi.org/10.1093/protein/12.3.203

Wang ZQ, Wang YS, Su ZG, 2013. Purification and characterization of a *cis*-epoxysuccinic acid hydrolase from *Nocardia tartaricans* CAS-52, and expression in *Escherichia coli*. *Appl Microbiol Biotechnol*, 97(6):2433-2441. https://doi.org/10.1007/s00253-012-4102-4

Waterhouse A, Bertoni M, Bienert S, et al., 2018. SWISS-MODEL: homology modelling of protein structures and complexes. *Nucleic Acids Res*, 46(W1):W296-W303. https://doi.org/10.1093/nar/gky427

Weng JR, Yang S, Shen JK, et al., 2023. Molecular dynamics simulation reveals DNA-specific recognition mechanism via c-Myb in pseudo-palindromic consensus of *mim-1* promoter. *J Zhejiang Univ-Sci B (Biomed & Biotechnol)*, 24(10):883-895. https://doi.org/10.1631/jzus.B2200634

Zhang Y, Geary T, Simpson BK, 2019. Genetically modified food enzymes: a review. *Curr Opin Food Sci*, 25:14-18. https://doi.org/10.1016/j.cofs.2019.01.002

Zhu WL, Sun HM, Jiang QX, et al., 2022. Enhancing the thermal stability of glutathione bifunctional synthase by B-factor strategy and un/folding free energy calculation. *Catalysts*, 12(12):1649. https://doi.org/10.3390/catal12121649

Supplementary information

Tables S1–S4; Figs. S1–S5